Patterns of spatial and temporal variability in streamflow records in south central Chile in the period 1952–2003

Eduardo Rubio-Álvarez[1] and James McPhee[1]

Received 16 March 2009; revised 29 September 2009; accepted 14 December 2009; published 14 May 2010.

[1] In this work we study the time series of annual and seasonal streamflow for 44 rivers in southern Chile, spanning the ecoregion between 34°S and 45°S for the 1952–2003 period. We analyze spatial variability using a clustering process to define regional streamflow averages. We find two main regions, divided approximately by parallel 37.5°S. The analysis includes application of the multitaper (MTM) and maximum entropy (MEM) methods to find periodicities or interannual and decadal cycles. Singular spectral analysis (SSA) is applied in order to augment the signal-to-noise ratio. Significant correlation with climatic indexes was found at different spatial and temporal scales, with El Niño–Southern Oscillation (ENSO) influence being stronger at the northern subregion, and notably the Antarctic Oscillation (AAO) and the Pacific Decadal Oscillation (PDO) showing strong correlation with summer flows in the southern subregion. Also, we found significant decreasing trends affecting a region between 37.5°S and 40°S. These are coherent with decreasing trends observed in precipitation in the area, and also with a decreasing trend observed in the Southern Oscillation Index (SOI). These findings provide, for the first time, a comprehensive view of the streamflow variability in a sensitive ecoregion in South America. We expect that these results will inform decision making in a context of increasing water demands for diverse uses as well as contribute to the general understanding of climatic patterns of variability in the Pacific Rim.

Citation: Rubio-Álvarez, E., and J. McPhee (2010), Patterns of spatial and temporal variability in streamflow records in south central Chile in the period 1952–2003, *Water Resour. Res.*, *46*, W05514, doi:10.1029/2009WR007982.

1. Introduction

[2] Water resources flowing from the western slope of the Andes Cordillera south of parallel 33°S constitute the cornerstone of Chile's agricultural and industrial activities, supply drinking water to more than half the Chilean population, and represent roughly 70% of the country's hydropower installed capacity [*Peña et al.*, 1999]. Because of its unique geographical location between the Andes Cordillera and the Pacific Ocean, the hydrologic regime of Chilean rivers is strongly modulated by the region's climate, with interannual variability following closely that of precipitation and with temperature controlling snow accumulation and melt processes in the high Andes. In turn, precipitation over most of central and southern Chile falls during winter (June–July–August (JJA)) months, when frontal systems stemming from the Antarctic storm track reach lower latitudes. During the past decade, there has been increased awareness within the scientific and engineering community regarding the high interannual and long-term variability affecting the precipitation and temperature regimes. Recent studies show a decreasing trend in precipitation for many stations throughout the country, together with increasing trends in temperature for those stations located in Chile's central valley and piedmont. The decreasing trend in precipitation is more pronounced in stations south of 38°S, and the temperature trends show opposite signs for coastal (negative) and inland (positive) stations [*Comisión Nacional de Medioambiente*, 2007; *Pezoa*, 2003].

[3] In this work we assess the degree to which already documented trends in climatic variability affect the hydrologic regime of rivers in the Chilean ecoregion located between parallels 34°S and 45°S, west of the Andes Cordillera. This is the first time in which a comprehensive streamflow data set of this spatial and temporal coverage is assembled and analyzed for this geographic region, and we build upon a number of studies that have improved the understanding of general climatic influences over the southern cone of South America [e.g., *Aravena and Luckman*, 2009; *Lara et al.*, 2008; *Masiokas et al.*, 2006, 2008; *Villalba et al.*, 2003]. We expect precipitation to have a strong influence on interannual variability, but the combined interplay of temperature gradients and physiography should introduce additional complexity in mixed-regime watersheds, which we attempt to uncover through the systematic analysis of a large database of unimpaired streamflow records. The specific objectives of our work include to define spatial and temporal patterns of streamflow variation representative of the period of record (1952–2003) and to identify, within these patterns, relationships with long-term climatic variability indexes as

[1]Departamento de Ingeniería Civil, Facultad de Ciencias Físicas y Matemáticas, Universidad de Chile, Santiago, Chile.

0043-1397/10/2009WR007982

well as with regional patterns of variation in precipitation and temperature.

2. Data and Methods

2.1. Area of Study

[4] The area of study spans the Chilean territory between parallels 34°S and 45°S, which includes what can be considered the central, south central, and the northern boundary of southern Chile. This region includes the basins of important river systems such as, from north to south, the Maule, Biobío, Imperial, Valdivia, Puelo, and Aysén rivers. Combined, these river systems represent roughly 9000 m^3/s, or 30% of the entire available mean annual streamflow in the country [*Peña et al.*, 1999]. Water uses include irrigated agriculture in the Maule and Biobío regions; hydropower generation, equivalent to more than 70% of the installed capacity in Chile (see http://www.cne.cl/cnewww/opencms/06_Estadisticas/energia/Electricidad.html); domestic and industrial water supply as well as important environmental services such as dilution of industrial liquid waste, plus freshwater for fisheries located in estuaries, lakes, and fjords south of 41°S.

[5] The regional climate ranges from Mediterranean in the northern extreme of the study area, to wet temperate to wet oceanic in coastal Patagonia. Annual rainfall averages from 500 to 5000 mm yr^{-1}, generally increasing southward with a strong shadow effect by the coastal range, which diminishes precipitation within the central depression and generates areas with heavy rainfall in the ecoregion denominated Valdivian temperate rain forest [*Pezoa*, 2003]. Precipitation variability is dominated by variations in the southeastern Pacific anticyclone [*Aceituno et al.*, 1993; *Pittock*, 1980], and El Niño–Southern Oscillation (ENSO) displays a dissimilar level of influence on interannual variability, with the northern portion of the study area being generally more sensitive to El Niño events than the southern subregion [*Aceituno*, 1988; *Montecinos and Aceituno*, 2003].

[6] An important factor modulating the streamflow regime in the study area is the Andes Cordillera. Within the study area, a transition zone develops, in which the elevation of the cordillera decreases, from approximately 3000 m above sea level (asl) at 34°S to less than 2000 m asl at 45°S. This transition combines with changes in temperature and precipitation along the latitudinal gradient producing rivers with different hydrologic regimes.

2.2. Stream Gage Data, Preprocessing, and Validation

[7] Basic data for this study consist of monthly streamflow records provided by the Ministry of Public Works's Dirección General de Aguas (DGA), which maintains the network of stream gages along the country. Data were initially gathered for 89 stations measuring unimpaired flow located between 34°S and 45°S in the administrative regions denominated (from north to south) Maule, Biobío, Araucanía, Los Ríos, Los Lagos, and Aysén. After filtering out those stations with less than 25 years of continuous period of record, and after verifying for consistency using traditional methods in hydrological analysis [*Searcy and Hardison*, 1960], we adopted a database of 44 stations. These data still presented gaps of varying length, which had to be filled through documented techniques such as regression with nearby stations, as well as monthly distribution curves obtained from the observed record, discriminating among dry (probability of exceedance greater than 66%), normal (probability of exceedance between 33% and 66%), and wet (probability of exceedance less than 33%), water years (in Chile, April through March). Because the objective of this study is to identify patterns of spatial and temporal variability, gap-filling efforts were limited in order to avoid duplicating excess information from one station to another. Where insufficient continuous information was available, the station was eliminated from the analysis. A special case was that of a group of stations located in the Los Ríos region, which consistently presented a shorter period of record (25 years) than that of the bulk of the stations (52 years). These stations were included in the analysis for the sake of maintaining an adequate spatial coverage, and were analyzed as explained later.

[8] Table 1 presents the stations included in this study and lists their location, average annual discharge, and coefficient of variation. Part of this information is also presented in Figure 1a. As seen in Figure 1a, data are spatially distributed somewhat uniformly between latitudes 35°S and 40°S. Many stations retained for the analysis are located at lower elevations, at the outlet of mountain valleys or within the central depression. Drainage direction for the majority of stations is from east to west. The lack of unimpaired flow records at higher elevations explains the relative scarcity of data near the international border with Argentina. Similarly, coastal watersheds are underrepresented because many of these streams do not constitute major sources of water supply and therefore are not monitored by DGA. South of parallel 40°S, the availability of streamflow data of sufficient quality decreases dramatically. Some stations do exist, but their period of record and data quality were considered insufficient for the purposes of establishing regional averages. Therefore only two stations (PCB and MJS, numbered 43 and 44 in Table 1) were included for this subregion, and their data were used solely for temporal variability analysis. Figure 1b also presents streamflow variability, expressed as the coefficient of variation of annual streamflow. The preliminary information provided by the coefficient of variation suggests two distinct zones of streamflow variability, divided approximately by parallel 38°S. North of this latitude we find stations with larger interannual, variability, with longer periods-of-record and in general with more data gaps. Between 38°S and 40°S, streamflow records are more complete and present smaller interannual variability but have shorter length (maximum of 25 years). This distribution of interannual variability with respect to latitude is very consistent with that suggested by *McMahon* [1982] and contributes to confirm those findings in what was, for the aforementioned study, an unsampled region of the world.

[9] Normalized annual (April through March) and seasonal mean flows (winter, April–September; and summer, January–March) were used in the analysis. Normalization is advantageous in this context because all stations are given equal weight and absolute-value bias is avoided, and also because the effect of precipitation magnitude and watershed contributing areas are equalized [*Wilks*, 2005].

Table 1. Stream Gages Included in the Analysis[a]

Number	Station Name	Latitude (deg)	Longitude (deg)	Annual Q (m^3/s)	Coefficient of Variation	Area (km^2)	Average Elevation (m above sea level)	Percent Q Winter	Percent Q Summer
1	Rio Perquilauquen En San Manuel	−36.42	−71.50	36	0.40	358	1305	63	4
2	Rio Longavi En La Quiriquina	−36.23	−71.47	47	0.33	669	1400	53	10
3	Rio Ancoa En El Morro	−35.90	−71.30	22	0.25	277	1374	48	20
4	Estero Upeo En Upeo	−35.18	−71.10	7	0.49	1412	2137	62	4
5	Rio Maule En Longitudinal	−35.57	−71.72	199	0.36	238	291	46	11
6	Rio Claro En Camarico	−35.17	−71.38	19	0.52	646	1037	59	7
7	Rio Perquilauquen En Quella	−36.02	−72.38	58	0.43	157	318	70	2
8	Rio Cauquenes En El Arrayan	−36.05	−72.08	8	0.62	1670	486	77	1
9	Rio Putagan En Yerbas Buenas	−35.78	−71.58	22	0.30	558	420	57	15
10	Rio Lirquen En Cerro El Padre	−37.78	−71.87	7	0.28	107	657	68	4
11	Rio Duqueco En Villucura	−37.55	−72.03	56	0.35	902	972	57	8
12	Rio Mulchen En Mulchen	−37.72	−72.25	21	0.30	417	469	64	6
13	Rio Bureo En Mulchen	−37.72	−72.23	42	0.30	545	666	66	5
14	Rio Malleco En Collipulli	−37.97	−72.43	29	0.32	420	811	65	5
15	Rio Ñuble En La Punilla	−36.65	−71.37	78	0.30	1434	1665	69	2
16	Rio Cato En Puente Cato	−36.55	−72.05	40	0.37	987	611	59	7
17	Rio Diguillin En San Lorenzo	−36.93	−71.57	17	0.30	196	1531	65	4
18	Rio Mininco En Longitudinal	−37.87	−72.40	16	0.32	702	826	67	3
19	Rio Itata En Balsa Nueva Aldea	−36.65	−72.45	136	0.38	4492	515	49	14
20	Rio Tolten En Villarica	−39.27	−72.23	272	0.20	2948	973	67	4
21	Rio Puyehue En Quitratue	−39.15	−72.67	7	0.26	145	207	59	8
22	Rio Puren En Tranaman	−38.03	−73.02	10	0.28	332	538	66	5
23	Rio Lumaco En Lumaco	−38.15	−72.90	18	0.34	539	252	53	12
24	Rio Cautin En Rari-Ruca	−38.43	−71.98	107	0.27	1201	1136	63	6
25	Rio Muco En Puente Muco	−38.62	−72.42	26	0.22	654	540	57	9
26	Rio Cautin En Cajon	−38.70	−72.52	144	0.23	2098	812	51	14
27	Rio Allipen En Los Laureles	−38.98	−72.23	142	0.21	1490	976	67	3
28	Rio Traiguen En Victoria	−38.22	−72.32	5	0.32	80	482	67	3
29	Rio Quepe En Vilcun	−38.68	−72.23	34	0.22	377	939	54	13
30	Rio Quillen En Galvarino	−38.40	−72.78	20	0.26	721	297	67	7
31	Bueno En Río Bueno	−40.22	−72.97	3724	0.13	437	179	50	15
32	Río Cruces En Rucaco	−39.57	−72.92	861	0.25	2572	409	65	6
33	Rïo Fui Antes Desague Neltume	−39.82	−72.00	1222	0.18	771	966	48	12
34	Fui En Des. Lago Pirihueico	−39.87	−71.90	874	0.26	1435	1180	48	8
35	Fui Arriba El Salto	−39.87	−71.92	839	0.24	1475	1172	49	8
36	Fui Bajo Junta Truful	−39.85	−71.97	1004	0.18	1552	1165	47	11
37	Huanehue En Des. L. Calafquen	−39.53	−72.12	673	0.16	736	734	47	16
38	Hum Hum En La Frontera	−40.08	−71.68	577	0.27	1063	1198	45	10
39	Hum Hum En Des. L. Pirihueico	−39.87	−71.90	638	0.21	1146	1193	46	11
40	Lipinza En Las Saleras	−39.95	−71.68	110	0.18	86	1332	48	9
41	Neltume En Des L. Neltume	−39.82	−72.02	886	0.16	770	966	58	10
42	San Pedro En Desague Lago Riñihue	−39.77	−72.47	4015	0.27	4214	914	53	12
43	Puelo En Carrera Basilio (PCB)	−41.62	−72.25	629	0.17	8718	1063	46	18
44	Mañihuales Antes Simpson (MJS)	−45.40	−72.47	176	0.19	4363	919	45	15

[a]Stations 1–30 and 43 with data for period 1952–2003. Stations 31–42 with data for period 1966–1990. Station 44 with data for period 1963–2006. Stations 43 and 44 not included in cluster analysis.

2.3. Spatial Analysis

[10] Identifying patterns of spatial variability involves the determination of geographical locations for which certain environmental variables display common features regarding distribution, temporal variability, extreme values, and the like. We applied clustering analysis to group the streamflow stations into homogeneous groups, which in turn we assumed represent homogeneous regions in terms of streamflow generation. This not an entirely rigorous concept, because streamflow generation even for closely located watersheds depends not only on the physical characteristics and meteorological forcings affecting a catchment but also on the scale of the watershed and its interaction with the physical processes that result in flow. However, here we assume that it might indeed possible to define a "homogeneous region" for streamflow production based on point measurements related to each other through the clustering process. The theoretical basis of the clustering method has been described in detail elsewhere [e.g., *Dettinger and Diaz*, 2000; *Kresch*, 1994; *Stahl and Demuth*, 1999a, 1999b], and therefore here we provide only the fundamentals of the application to the streamflow database. Each station's time series is seen as a column vector in a matrix with nstation columns and mtimes rows. Each column is normalized by its mean and standard deviation, and the distance between each pair of columns is computed using a norm. Two "close" columns are grouped together, and the distance between this group and the remaining columns is computed, so if the distance between a group and a vector is small enough, then the vector becomes part of the group. Intuitively, the records that are closest together are grouped first, so that the minimum distance between any station and an existing group increases at each successive grouping stage. A closing criterion is needed therefore to decide when to stop grouping variables. *Fovell and Fovell* [1993] suggest that Monte Carlo analysis can be used to determine the distance at which continued clustering

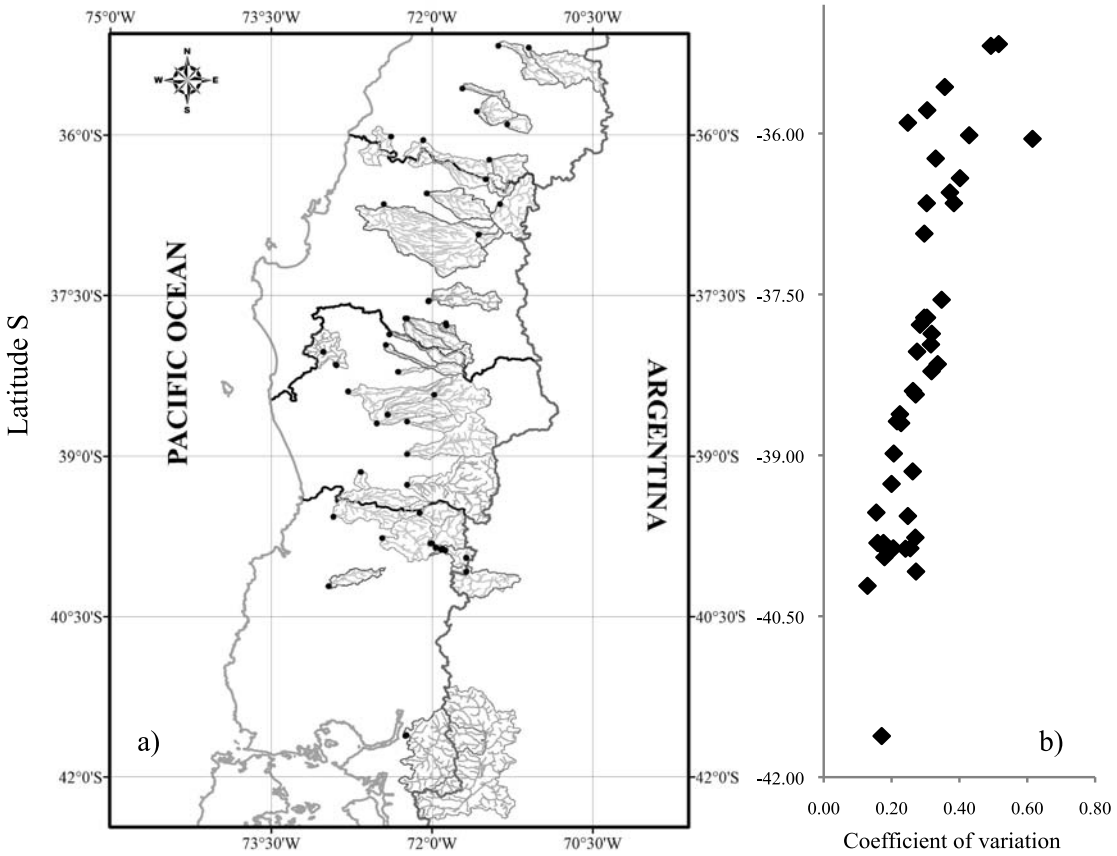

Figure 1. (a) Stream gage location, basin delineation, and river network. (b) Coefficient of variation as a function of latitude. Variability decreases as latitude increases within the study area.

ceases to be meaningful, but *Wilks* [2005] proposes a graphical method, in which a metric of the distance between the clusters and the next available vector is plotted versus the number of already grouped vectors. The point at which there is an abrupt change in the slope of this curve should be selected as the stopping level of aggregation. By and large, the stopping aggregation level remains a subjective decision, and judgment should be applied, by always verifying the physical significance of the obtained clusters.

[11] In this study, a special situation arose due to the fact that a specific subset of streamflow records, corresponding to the newly created Los Rios region (stations 32–42 in Table 1), present consistently shorter periods of record. The longest concurrent period of record with the remaining stations that could be achieved without recurring to inordinate amounts of gap filling was 25 years, from 1966 to 1990. In order to include these stations in the clustering process, we carried out a sensitivity analysis of the clustering results by separating the 52 year period of the remaining stations into three windows: 1952–1975, 1966–1990, and 1975–2003. We performed the clustering analysis for each window and verified the robustness of the method, i.e., that very similar clusters result from using the three time windows. We used different linkage methods and norms in order to test the stability of the resulting clusters, and we evaluated the quality of the association using the cophenetic correlation coefficient. By these criteria, we chose to retain the clusters obtained by the combination of a Minkowski norm and an averaging linkage method, although the Euclidian norm yielded also results that were indistinguishable from the best combination. Because of space restrictions these results are not shown. In consequence, we conclude that it is possible to apply clustering to the entire group of 42 stations (not including stations 43 and 44, because of their geographical location, approximately 500 km south of the closest stream gage in the data set in the case of station 44) using only a 25 year record, in order to obtain representative spatial patterns of variation. Then the obtained spatial patterns can be used to compute regional normalized streamflow averages, this time using only those stations with the entire 52 year record, for time variability analysis.

2.4. Temporal Variability

[12] The resulting normalized, regionally averaged annual and seasonal streamflow time series obtained from the clustering process were assessed in search of consistent patterns of temporal variability. This included trend analysis and a search for significant oscillatory cycles that may explain variability at decadal and subdecadal scales, taking into account the restricted length of the period of record. We augmented the signal-to-noise ratio of the streamflow regional averages using singular spectral analysis (SSA) and then estimated the periodogram of each SSA-reconstructed

time series by a two-step procedure, whereby the multitaper method (MTM) is applied to identify significant oscillatory periods and the maximum entropy method (MEM) is used to verify the robustness of the MTM estimation. The details of these methods have been documented intensively [e.g., *Allen and Smith*, 1996; *Dettinger et al.*, 1995; *Ghil et al.*, 2002; *Mann and Lees*, 1996; *Vautard et al.*, 1992] and therefore are not repeated here. Essentially, first SSA was applied to the original time series of composite streamflow anomalies, and a reconstructed time series (reconstructed component, or RC) was obtained by retaining a subset of the eigenvectors of the Toeplitz matrix of observed anomalies. The choice of eigenvectors or empirical orthogonal functions (EOFs) to keep in the reconstruction process is intended to increase the signal-to-noise ratio, and significant pairs of eigenvectors are identified by applying the same frequency and strong fast Fourier transform (FFT) tests [*Vautard and Ghil*, 1989]. Subsequently, we estimate the periodogram of the SSA-reconstructed time series using two independent methods. MEM [*Penland et al.*, 1991] is based on approximating a time series by an autoregressive (AR) process of order M, where M is the length of the time window used in scanning the data; it is a parametric method, in which the estimated parameters are the multiplying coefficients of harmonic functions that constitute the spectral density function at different frequencies. Unlike MEM, MTM is a nonparametric method that premultiplies the data by orthogonal tapers built to minimize the spectral leakage that arises from the finite length of the data set. The tapers are computed from the data set by solving a Rayleigh-Ritz minimization problem, as detailed by *Thomson* [1990] and *Percival and Walden* [1993]. In both methods, important considerations include the choice of length of the window used in estimating the autocorrelation function, and its relation to the number of available observations. We used a 10 year window length (M) for the analysis of the 1952–2003 time series, and M = 8 years for the MJS station (numbered 44 in Table 1, it has a shorter record, spanning the 1963–2003 period), which are consistent with the criteria presented by *Vautard and Ghil* [1989] and *Ghil et al.* [2002].

[13] Finally, we evaluate the relative influence of known climatic patterns by computing the correlation coefficients between the regional streamflow averages and ENSO [*Smith et al.*, 2008], Pacific Decadal Oscillation (PDO) [*Zhang et al.*, 1997], Antarctic Oscillation (AAO) [*Thompson and Wallace*, 2000], as well as Southern Oscillation Index (SOI) [*Ropelewski and Halpert*, 1989]. Each index was computed from original monthly values for the same temporal aggregation period applied to the streamflow series, i.e., annual (April–March), winter (April–September), and summer (January–March of the following year).

3. Results and Discussion

3.1. Spatial Patterns of Variability: Cluster Analysis

[14] Figure 2 shows the clustering results for the annual streamflow anomalies time series. We found two large groups of stations, which we have called "north" (numeral 1) and "south" (numeral 2) clusters. The north cluster includes most stations located in the great Maule River watershed, and some stations at the northern edge of the Biobío region, although one station within the Biobío region also results grouped in this cluster. The south cluster includes most stations within the Biobío region, plus stations in the northern edge of the Araucanía region (north of parallel 40°S). In delineating the regional patterns shown in Figure 2, we have attempted to reconcile the numerical results of the clustering method and physical meaningfulness of the regionalization. Therefore some stations that were not grouped with the larger clusters (which are shown at the far right edge of Figure 3a) are nevertheless shown within the hand-drawn limits of these. Figure 3b illustrates the criterion used to stop the grouping process, in which the threshold distance between merged clusters (approximately 3.0) corresponds to a change in slope of the distance versus stage curve. This method of supervised classification relies on a subjective definition of when a change in slope merits stopping of the clustering process; as such, the final clusters depend on human judgment. Stations Puelo en Carrera Basilio (PCB, shown in Figure 2a as the lowermost dot) and Manihuales antes Junta Simpson (MJS, not shown in Figure 2) are special cases in that they are analyzed as individual time series, despite the fact that the clustering method did not result in them being included within any homogeneous streamflow zones. We justify this decision on these stations being the only ones with long enough period of record and sufficient data quality within the southernmost part of the study area.

[15] Figures 4a and 4b show results of the clustering method applied to winter and summer flow anomalies. In this case, "summer" is defined as spanning the January–February–March (JFM) period only, after analysis of a 6 month period from September through March resulted in many clusters consisting on few stations each, and with many overlapping regions among different clusters; this result was considered not meaningful from a hydrologic standpoint, as we would expect dry-season flow to be consistent with precipitation and temperature regimes, modulated by watershed elevations. A first comment that arises from inspecting Figure 4a is that winter flow patterns correspond almost exactly to those of annual flow, indicating that interannual variability is strongly determined by winter streamflow. This is true even for the northern stations, which are located in a geographic region where the Andes Cordillera is higher, and therefore present hydrologic regimes more strongly dominated by spring and summer snowmelt. As in Figure 2, two regions are clearly defined, with the boundary located at approximately 37.5°S. The presence of this boundary is strikingly coincident with the "zero boundary" found in the second principal component (PC) for annual and seasonal precipitation during the 1962–2000 period reported by *Pezoa* [2003]. This PC accounts for between 10% and 15% of precipitation variability depending on the seasonal averaging, and displays a decreasing trend at the annual, spring, and fall aggregation levels.

[16] The summer grouping, shown in Figure 4b, shows a well defined southern cluster including most stations in the Biobío region plus the available stations in the Araucanía and Los Rios region (labeled with the numeral 4). The northern boundary of the south cluster again matches approximately the "zero boundary" found for the second PC of precipitation data presented by *Pezoa* [2003]. Remarkably, the north cluster does not appear at this aggregation level. Instead, smaller groups of stations appear, such as those indicated with the numerals 2, 6, and 9. The stations

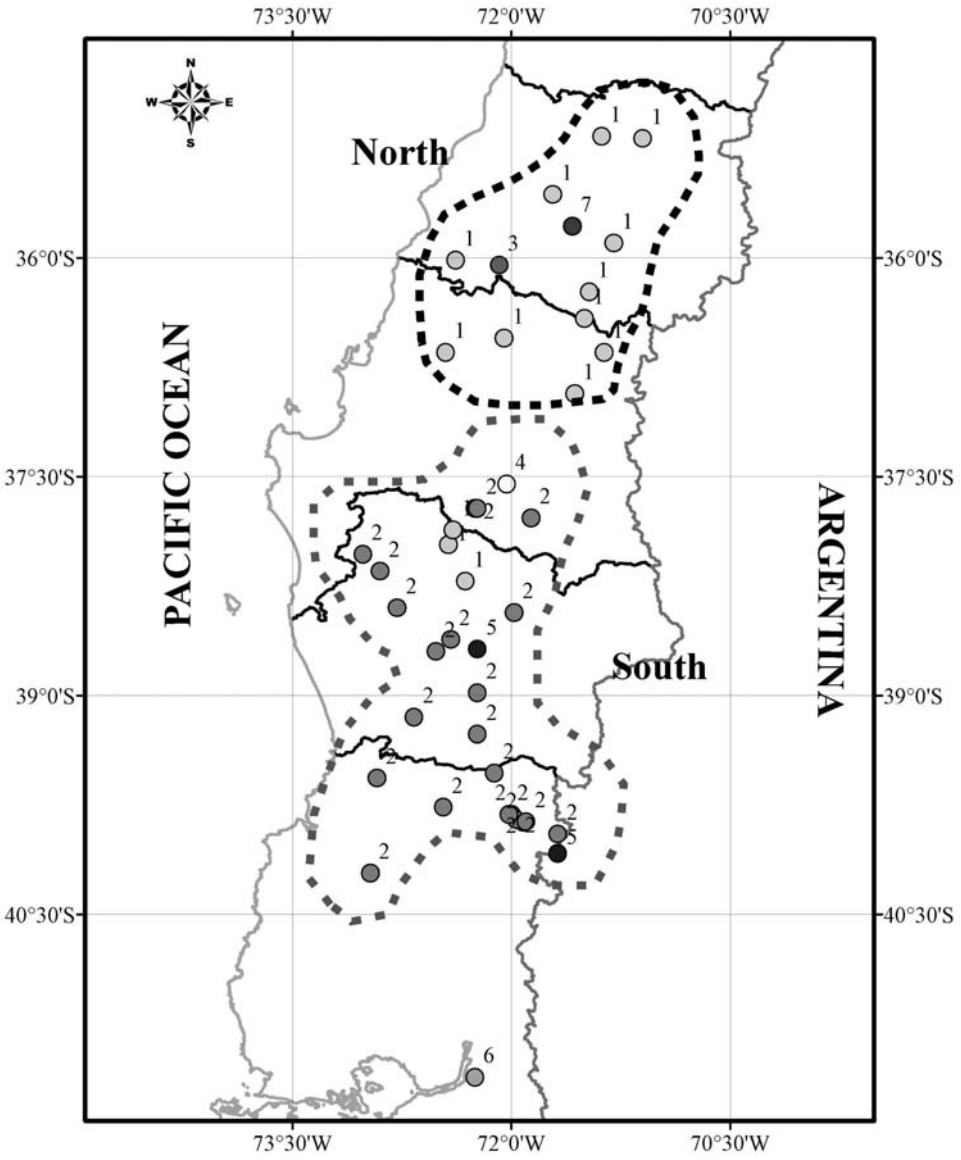

Figure 2. Cluster results for 43 stream gages, mean annual flow, period 1966–1990. Spatial clusters from annual streamflow anomalies are delineated by hand; numerals labeling each station correspond to cluster number. Stream gage MJS is not shown.

belonging to these smaller clusters correspond to different watersheds, are located both close to the coast and at higher elevations, and in general do not present a common set of hydrologic features that could lead to an intuitive grouping of their summer streamflow. On addition, from Figure 1 it can be seen that many of the stations in this region present the highest degree of variability. In summary, we conclude that only the south cluster is reliable for summer flows and include only the latter regional average, plus stream gages PCB and MJS, in the analyses below.

3.2. Temporal Variability

3.2.1. Relationship With Climatic Indexes

[17] Table 2 presents the corresponding correlation coefficient R, and p-value for different combinations of climatic forcings and streamflow series. We present in bold face the significant correlation coefficients at 95% confidence level. The first group of results shows that annual flows for the north and south clusters are positively correlated with ENSO 3.4 and negatively correlated with SOI. The two stations located farther south in the study area do not show a significant relation with ENSO and SOI, which is consistent with the fact that the influence of these two indexes over precipitation diminishes consistently with south latitude. We also verify that AAO is negatively correlated with annual flows, and that this relation is robust for annual and winter values of AAO south of 37°S and even for summer AAO for the MJS stream gage. The negative correlation in the case of the MJS station contributes to strengthen the annual correlation and is explained by the fact that in this region, summer precipitation and snowmelt contribute significantly to river flows (see Table 1).

[18] When focusing on winter flows, the influence of ENSO and SOI, with different signs, expands to the Puelo River (PCB) such that positive ENSO phases are related to

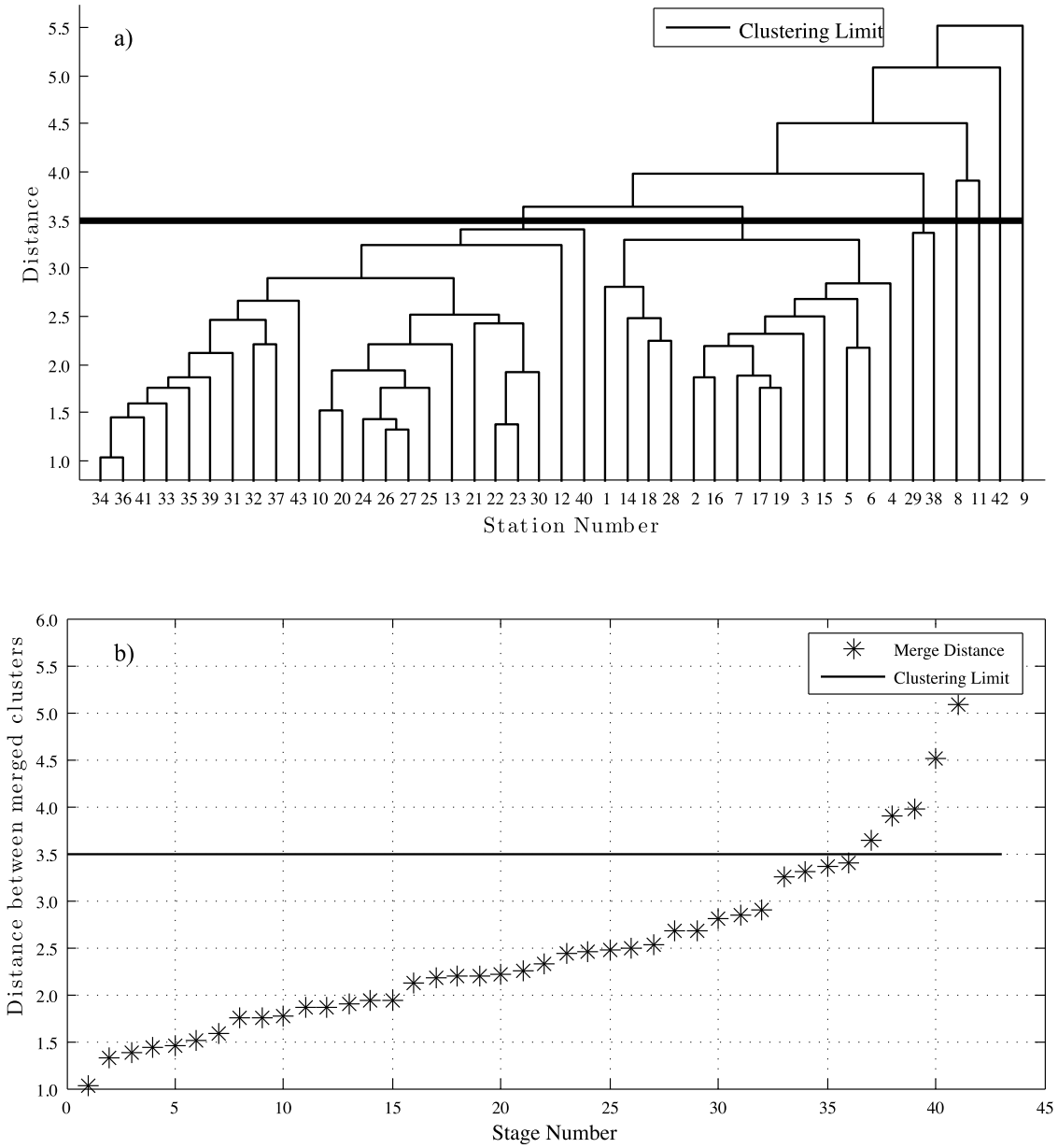

Figure 3. (a) Hierarchy tree resulting in spatial patterns shown in Figure 2. (b) Distance between merged clusters versus stage number in clustering process. Solid line indicates stopping threshold.

larger winter flows with correlation in the order of 0.3. AAO is negatively correlated to the south cluster and with the MJS station, but not to the north cluster nor to the PCB station. Finally we see strong negative correlations between summer flows for the south cluster, i.e., stations in south central Chile and same season as well as previous winter PDO and AAO values. Puelo River (PCB) summer flows are positively correlated to previous-season SOI and are therefore negatively related to previous-season ENSO. For coastal Aysén (MJS station), we find significant positive correlation with same-season SOI but negative correlation with previous-season PDO.

[19] *Verdon and Franks* [2006] use proxy climate records derived from paleoclimatic data to investigate the long-term behavior of ENSO and PDO. They find that the positive phase of PDO (or IPO) is associated with increasing frequency of El Niño events (warm ENSO episodes) and that the negative phase of PDO is a favorable condition for the development of La Niña events (cold ENSO episodes). Hence, according to the results shown in Table 2 there is a negative correlation between PDO and the summer patterns flows so that during a negative phase of PDO, we expect increased summer streamflow south of the Maule River basin, associated with a possible reduction in the values of ENSO according to the *Verdon and Franks* [2006] hypothesis. However, given the positive correlation between ENSO and winter (as well as annual, although less intense and widespread) streamflow throughout the area of study (Table 2), we can also expect diminished winter flows under negative PDO conditions. Combined, these two results imply that intense negative phase of PDO would result in less overall flow and a shift to summer discharge for an extended geographical region between the Maule and Puelo river basins. The same pattern is observed for the MJS station, but

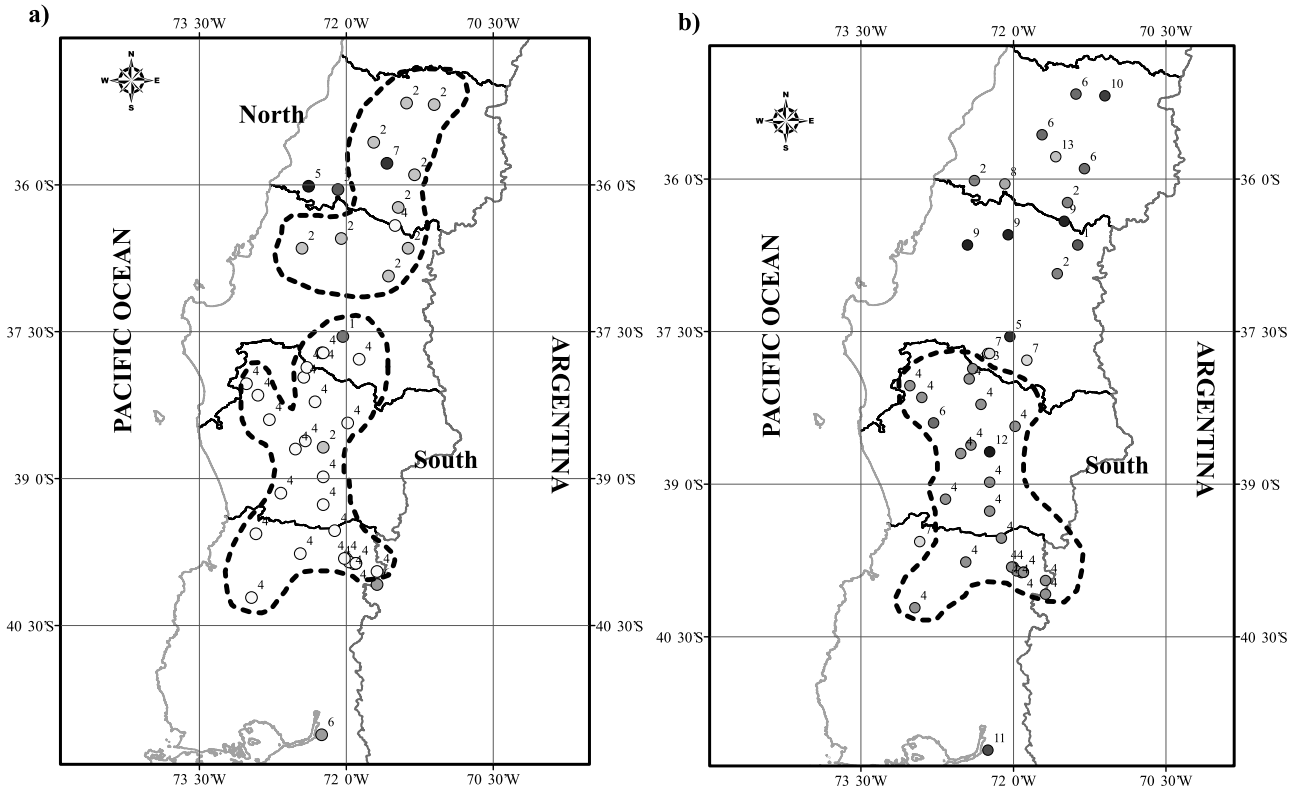

Figure 4. Streamflow clusters for (a) average winter flow anomalies (April through September) and (b) average summer flow anomalies (January through March). Clusters are delineated approximately, in order to convey spatial coherence. Stream gage MJS is not shown.

Table 2. Correlation Coefficients Between Annual Regional Streamflow and Climatic Indexes for the 1952–2003 Period[a]

	Add Heading	ENSO 3.4			PDO			AAO			SOI		
		Annual	Winter	JFM	Annual	Winter	JFM	Annual	Winter	JFM	Annual	Winter	JFM
Annual													
North	R	**0.503**	**0.515**	**0.422**	0.203	0.118	(0.243)	−0.191	(−0.243)	−0.078	**−0.534**	**−0.570**	**−0.382**
	p	**0.000**	**0.000**	**0.002**	0.149	0.406	(0.083)	0.176	(0.083)	0.583	**0.000**	**0.000**	**0.005**
South	R	**0.368**	**0.373**	**0.306**	0.114	0.077	0.092	**−0.291**	**−0.364**	−0.112	**−0.425**	**−0.464**	**−0.293**
	p	**0.007**	**0.007**	**0.027**	0.421	0.588	0.518	**0.037**	**0.008**	0.428	**0.002**	**0.001**	**0.035**
PCB	R	(0.263)	0.216	0.240	−0.107	−0.128	−0.046	**−0.299**	**−0.313**	−0.221	(−0.258)	(−0.257)	−0.191
	p	(0.065)	0.132	0.094	0.461	0.376	0.752	**0.035**	**0.027**	0.124	(0.071)	(0.072)	0.184
MJS	R	0.125	0.108	0.090	−0.194	−0.182	−0.125	**−0.493**	**−0.439**	**−0.379**	−0.042	−0.033	−0.007
	p	0.437	0.501	0.577	0.223	0.254	0.436	**0.001**	**0.004**	**0.015**	0.793	0.836	0.968
Winter													
North	R	**0.506**	**0.518**	…	**0.273**	0.189	…	−0.060	−0.131	…	**−0.536**	**−0.571**	…
	p	**0.000**	**0.000**	…	**0.050**	0.179	…	0.671	0.354	…	**0.000**	**0.000**	…
South	R	**0.308**	**0.332**	…	0.120	0.110	…	−0.224	**−0.338**	…	**−0.370**	**−0.415**	…
	p	**0.026**	**0.016**	…	0.396	0.440	…	0.111	**0.014**	…	**0.007**	**0.002**	…
PCB	R	**0.397**	**0.352**	…	0.006	0.012	…	−0.114	−0.198	…	**−0.364**	**−0.372**	…
	p	**0.004**	**0.010**	…	0.967	0.931	…	0.423	0.160	…	**0.008**	**0.007**	…
MJS	R	0.258	0.236	…	−0.017	0.034	…	(−0.295)	**−0.337**	…	−0.189	−0.176	…
	p	0.103	0.137	…	0.917	0.834	…	(0.061)	**0.031**	…	0.236	0.271	…
JFM													
South	R	−0.058	−0.096	0.006	**−0.366**	**−0.375**	**−0.318**	**−0.520**	**−0.389**	**−0.556**	0.064	0.082	0.054
	p	0.682	0.500	0.967	**0.008**	**0.006**	**0.022**	**0.000**	**0.004**	**0.000**	0.650	0.565	0.706
PCB	R	**−0.318**	**−0.308**	(−0.263)	**−0.409**	**−0.443**	**−0.369**	**−0.398**	**−0.319**	**−0.422**	**0.327**	**0.305**	(0.270)
	p	**0.022**	**0.026**	(0.060)	**0.003**	**0.001**	**0.007**	**0.004**	**0.021**	**0.002**	**0.018**	**0.028**	(0.053)
MJS	R	−0.236	−0.217	−0.219	**−0.316**	**−0.337**	−0.207	−0.221	−0.113	(−0.279)	**0.312**	0.244	**0.313**
	p	0.138	0.174	0.170	**0.044**	**0.031**	0.194	0.165	0.484	(0.077)	**0.047**	0.125	**0.047**

[a]MJS for 1963–2003 period. Bold face values are significant at 95% confidence level. Values in parentheses could be significant at lower confidence levels (>90%). PDO, Pacific Decadal Oscillation; AAO, Antarctic Oscillation; SOI, Southern Oscillation Index.

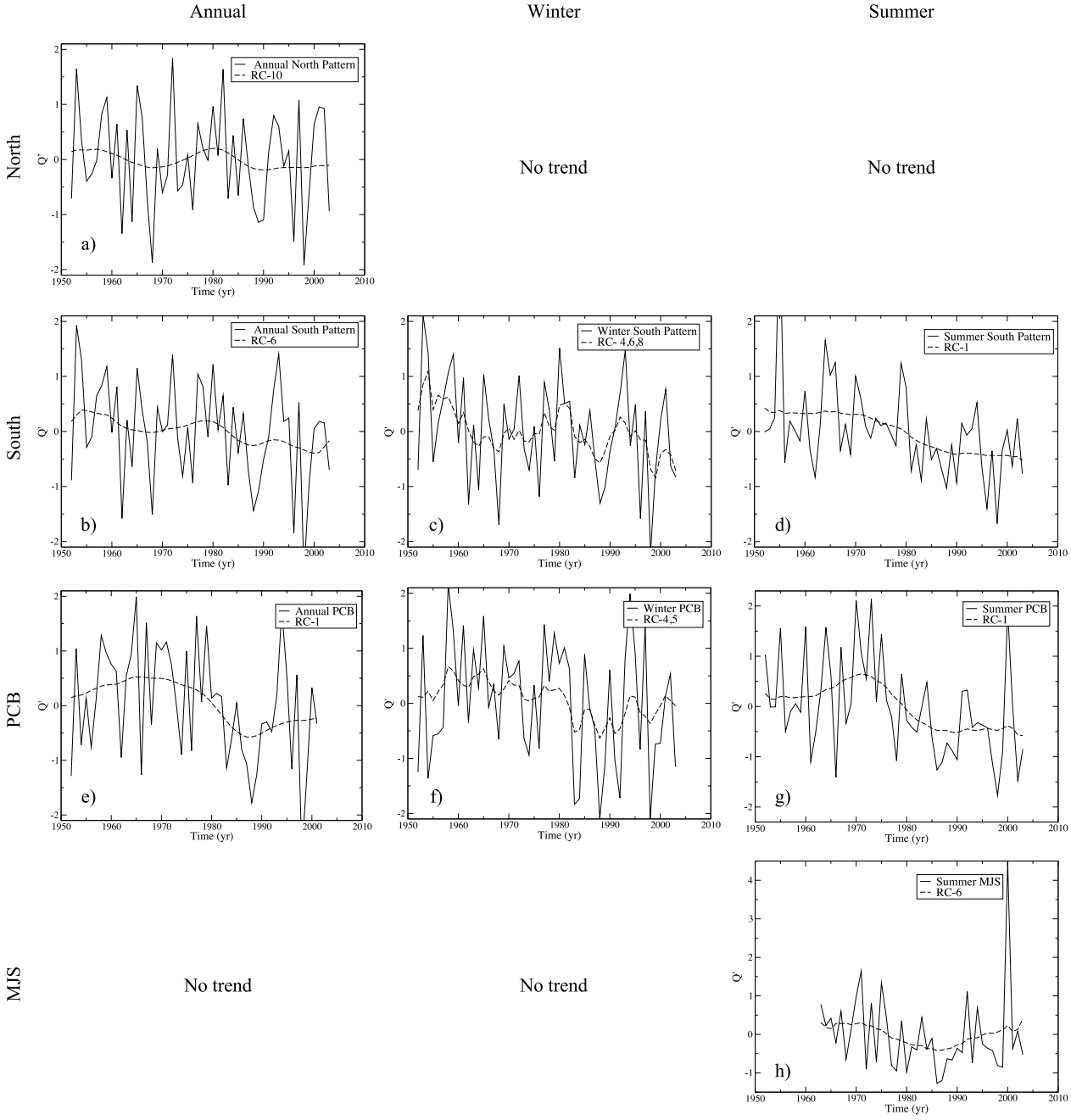

Figure 5. Significant trends found through Singular spectral analysis (SSA) decomposition of annual and seasonal streamflow series. Trends are significant at a 95% confidence level according to the Mann-Kendall nonparametric test applied to individual principal components.

this result is less conclusive from a statistical standpoint. From another point of view, if we look at the results shown in Table 2 in terms of summer regional discharge, it is interesting to note that the effects of PDO appear to be localized in two different zones (from a statistical standpoint). Summer PCB shows the strongest correlation with PDO and also is the only flow series showing a statistically significant relation with ENSO. However, MJS is positively correlated with SOI and weakly correlated with ENSO. It is usually accepted that SOI and ENSO are correlated, so the fact that MJS and SOI are significantly related could hint at ENSO having an extended area of influence farther south from central Chile.

3.2.2. SSA Decomposition and Trend Analysis

[20] Figure 5 shows the reconstructed trend and original, unfiltered series, and Table 3 presents a summary of significant oscillatory and trend components for each streamflow series. In Figure 5, the top two rows represent the different regional streamflow averages identified through clustering analysis, and the bottom two rows correspond to the individual gages PCB and MJS. Columns present the different levels of temporal aggregation. First, in terms of annual flows we see significant trends identified for the north, south and PCB series (Figures 5a, 5b, and 5e). These trends show different features: The stronger trends are those

Table 3. Significant Oscillatory Periods, Eigenelements, and Trend Components Resulting From SSA-MTM, MEM Analysis[a]

	Period					Pairs of Eigenelements			Trend Component		
Regional Flow Index	1	2	3	4	5	1	2	3	1	2	3
Annual											
North	5.95	2.42	…	…	…	(2,4)	…	…	10	…	…
South	5.95	3.61	2.01	…	…	(2,3)	(9,10)	…	6	…	…
PCB	4.21	2.32	…	…	…	(5,6)	(9,10)	…	1	…	…
MJS	6.69	3.08	…	…	…	(3,4)	(7,8)	…	1	…	…
Winter											
North	6.61	…	…	…	…	(1,2)	…	…	…	…	…
South	6.83	3.37	…	…	…	(2,3)	(9,10)	…	4	6	8
PCB	11.38	6.10	4.02	…	…	(1,2)	(4,5)	…	4	5	-
MJS	7.59	3.03	…	…	…	(1,2)	(5,6)	…	…	…	…
Summer (JFM)											
South	9.39	5.00	3.02	2.61	2.14	(2,3)	(4,5)	(6,7)	1	…	…
PCB	8.13	**4.65**	4.49	2.88	**2.69**	(2,3)	(4,5)	(7,8)	1	…	…
MJS	4.97	…	…	…	…	(2,3)	…	…	6	…	…

[a]Periods are significant at the 99% confidence level against a red-noise null hypothesis, except for boldface values, which are significant at 95% confidence level.

obtained for the south and PCB series, and the latter shows a distinct "rebound" behavior during the last decade of the twentieth century. This rebound is associated with the winter trend (Figure 5f), which not only displays this feature but also includes a cyclic component with a 6 year period. The shape of the reconstructed annual trend component for PCB is very similar to that of the reconstructed SOI series presented by *Ghil et al*. [2002], with an increasing phase lasting until approximately 1970, then a sudden drop lasting for about 10 years, and then a weaker trend during the last decade of the twentieth century. In comparison, the winter trend for the south series is much stronger than that of PCB, and also displays a cyclic component. The summer season series (Figures 5d, 5h, and 5i) also shows a decreasing trend for the south, PCB, and MJS series. It is interesting to note that the decreasing trend component does show a marked strengthening during the decade of 1970, to weaken in subsequent years. In MJS, the summer trend shows a similar "rebound" as the annual and winter trends in PCB, suggesting that there is a lagged effect influencing these two watersheds, separated by 500 km approximately. The timing of the trend reversal for PCB and MJS (around 1990) is approximately coincident with a noticeable change in the trend of PDO annual average from a strong increase to an oscillatory, decreasing trend [see *Chen et al.*, 2008].

3.2.3. MTM and MEM Periodogram Estimation and Series Reconstruction

[21] The streamflow series were reconstructed using significant pairs of principal components obtained through SSA. These reconstructed series were analyzed with the multitaper method (MTM), and the identified oscillatory periods were verified using the maximum entropy method (MEM). All MTM-identified periods were validated by MEM. Because of space limitations, in Figure 6 we show only one example of the applied methodology. Figure 6a presents the singular spectrum of the annual south regional flow index. From the strong FFT and same frequency criteria, two pairs of significant eigenelements are identified, namely, 2–3 and 9–10. Figures 6b and 6c show the MTM spectrum for the RCs associated with these two pairs of eigenelements. It can be seen that at 99% confidence levels, all four frequencies are identified as harmonic against a red-noise null hypothesis. Figure 6d shows the MEM spectrum for the SSA-reconstructed series resulting from the two pairs of eigenelements indicated above. The three main cycles identified by MTM (0.15, 0.26, and 0.48 cycles/yr) are also present in the MEM spectrum. This is also true for all other series and time periods (not shown).

[22] Table 3 summarizes the results obtained for this part of the analysis. A 2 year cycle is found for the north, south, and PCB annual and summer series, suggesting that at this frequency, interannual variability is strongly influenced by dry season discharge. A second group of periods, between 3 and 6 years, appear for all regional streamflow averages at different temporal aggregation levels. In particular a quasi-quadrennial period appears only for the annual, winter, and summer PCB series. The quasi-biennial and quasi-quadrennial periods have been associated to ENSO, and also are related with in tropical SSTs and zonal winds over the Pacific Ocean [*Robertson and Mechoso*, 1998]; with respect to the significant 6 year period shown in Table 3, this has been related with North Pacific SSTs [*Robertson*, 1996].

[23] The longer periods, of approximately 7, 8, 9, and 11 years, are found for series south of 37°S, with the lengthiest of these being associated with winter PCB streamflow. The period of 11.38 years is quite larger than the window length (M = 10) adopted for the analysis. However, the frequency associated to this spell is 0.088 cycles/yr. Considering that our Rayleigh frequency is $1/N = 1/52 = 0.019$ cy/yr, for the MTM method the frequency bandwith is $p \times f = 3 \times 0.019 = 0.058$ cy/yr, which represents the minimum frequency that MTM can detect. Therefore, although this frequency satisfies the main criteria for this method, and also is detected (not shown) for MEM spectrum, it represents a spell that may not be accurate due to its value, close to the length of the MTM window for this series. In view of the correlation analysis results shown below (Table 2) we believe that these long (near-decadal) periods found in summer flow could be related to the PDO and AAO indexes. Further research is needed on the spatial correlation structure of flows and climatological variables in order to ratify this assertion.

[24] Also, for the winter PCB time series, SSA identified the eigenelement pair (4,5) as a significant possible oscillatory mode (not noisy) with a 6.1 year period. On the other hand, the Mann-Kendall test yields that the trend present in the time series is also associated with this eigenpar. Therefore, by removing the trend for MTM analysis, we also are

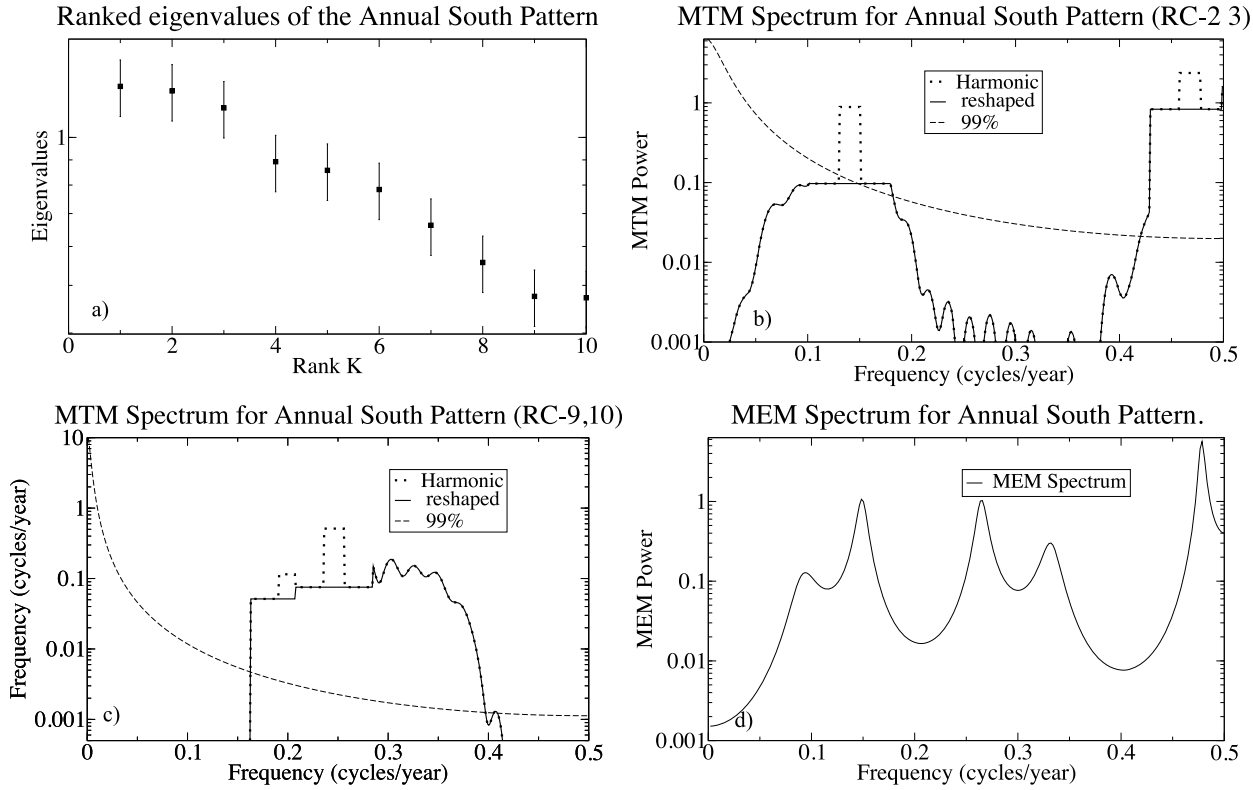

Figure 6. Example of application of SSA, multitaper (MTM), and maximum entropy (MEM) to annual streamflow index corresponding to the south subregion. (a) Ranked eigenvalues from SSA analysis; components 2–3 and 9–10 are significant and retained for variability analysis. (b and c) Multitaper periodogram estimation based on reconstructed components 2–3 and 9–10, respectively. (d) Maximum entropy periodogram estimation. Significant cycles in Figures 6b and 6c match those shown in Figure 6d.

losing this possible 6.1 year spell. The trend found in the winter PCB series may indicate several things (Figure 5f). For example, the trend component itself shows a distinct behavior before and after 1983, with a decreasing period leading to an increasing phase. Also, the trend shows a significant oscillation period so we might expect future increases of winter streamflow, modulated every 6 years. Of course, this is relatively short-term behavior that could very well be modulated by much larger scale oscillatory patterns, as shown by *Lara et al*. [2008].

[25] Figures 7, 8, and 9 present the MTM-reconstructed time series of significant RCs for every regional streamflow average for summer, winter, and annual aggregation levels respectively. For the south cluster, we note a decrease in the amplitude of the RC 2–3 oscillation, which occurs approximately in 1975 (Figure 7a). After 1985, the amplitude of this signal stabilizes at approximately one half standard deviation. For the other two RC pairs, we see again periods of relatively high amplitude at the beginning of the series, followed by periods of a more subdued behavior between 1970 and 1990, finishing with increased variability in the last 10 years (Figures 7b and 7c). The two southernmost stations within the area of study show a different behavior. We still observe variations in amplitude for each reconstructed component, but for PCB they are slighter than for the south pattern (Figure 7d) and occur out of phase with the latter, such that the 4–5 RC shows increased variability between 1965 and 1980, and smaller amplitudes thereafter (Figure 7e). The summer MJS time series yielded only one significant eigenpar (RC 2–3, in Figure 7g), and this component behaves somewhat similarly to the south RC 2–3 series, with 15 year intervals of high, low, and high variability.

[26] For winter flows, the north cluster shows a slight decrease in variability starting from 1975 (Figure 8a). Farther south we find indication of a possible relation between streamflow variability and the behavior of large-scale climatic patterns. In Figure 8b a decrease in variability can be appreciated between 1970 and 1985, and a return to increased amplitude after 1990. This pattern is coincident with a sequence of negative and positive phases in PDO. A similar behavior can be seen for MJS, although in this case the transition is defined by a smooth (Figure 8f) and an abrupt pattern (Figure 8g) that closely replicate phase changes of the PDO. As suggested by *Verdon and Franks* [2006], positive phases in PDO are correlated with increased ENSO activity, in particular with El Niño events. This would explain a more active winter streamflow series for the south and PCB patterns, and the fact that although PCB and PDO are not strongly correlated (Table 2), influence of the latter would be felt through the relationship with ENSO. For MJS, however, there is no significant correlation with ENSO or PDO; from Table 2 we see that winter MJS flow is negatively correlated with winter and annual AAO, which has experienced increased phase shifts after 1990, in

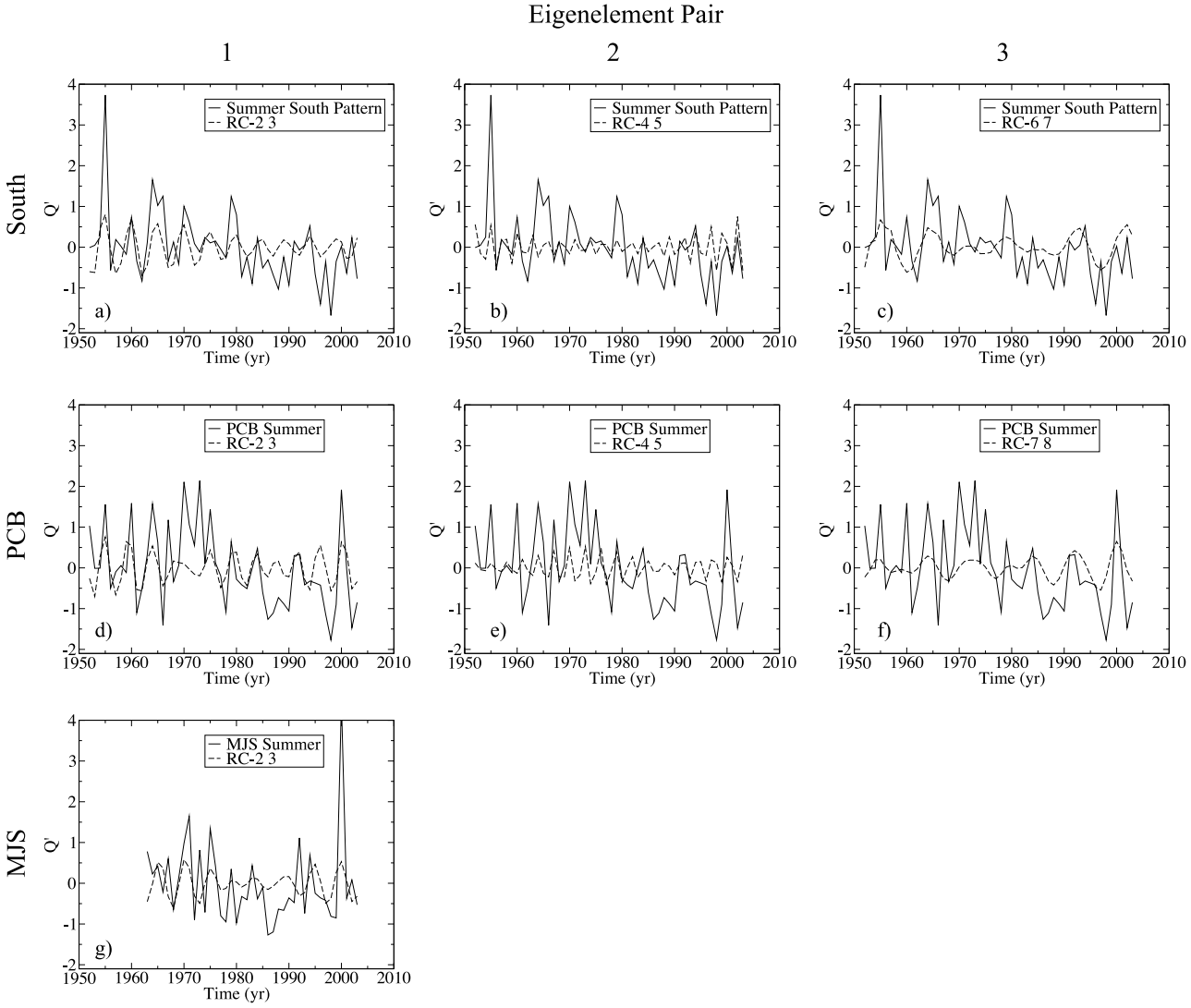

Figure 7. MTM reconstruction of SSA reconstructed components (RCs) for annual regional streamflow composites resulting from cluster analysis. Solid line shows original time series, and dashed line shows reconstruction based on pair of RCs as indicated in legend.

effect generating a quasi-biennial cycle that could be affecting river flows at higher south latitudes.

[27] Finally, at the annual aggregation level we see results that suggest that seasonal variability patterns do not cancel out, but instead reinforce each other. For the north cluster (Figure 9a), amplitude in the reconstructed RC 2–4 series is reduced approximately by one half after the mid 1970s, whereas for the south cluster this phenomenon is slighter (Figure 9b) while increased variability after 1990 can be seen in the RC 9–10 reconstruction (Figure 9c). For the Puelo River station (PCB), the reconstructed RC 5–6 pair also shows a shift (decreasing) in amplitude, but this occurs at a later date, around 1980 (Figure 9d), and is followed by increased variability at a larger frequency from approximately 1985 (Figure 9e). For the Mañihuales River station (MJS), for summer flows we identify three periods with distinct behavior (Figure 9f), although the length of record is insufficient for concluding emphatically. Figure 9g shows that the RC 7–8 reconstruction captures the same pattern identified for winter flows, which suggests a significant phenomenon affecting winter streamflow (precipitation contribution to annual volume) related somehow to AAO through the increased variability displayed by this climatic forcing starting in the last decade of the twentieth century.

4. Conclusions

[28] A myriad public policy and private decisions, such as land use planning and development, strategic decisions on government support for productive sectors such as forestry, aquiculture, and agriculture, private investment in hydropower and other areas, etc., are sensitive to current and future availability of water resources in the quantity, timing, and quality required for these objectives. In Chile, these questions acquire special relevance because of increased pressure on land and water resources by agricultural, logging, fisheries, and hydropower projects. In this paper we present a comprehensive analysis of current patterns of streamflow variability for a significant portion of the Chilean territory and suggest possible future scenarios in view of projected changes in regional and global climate.

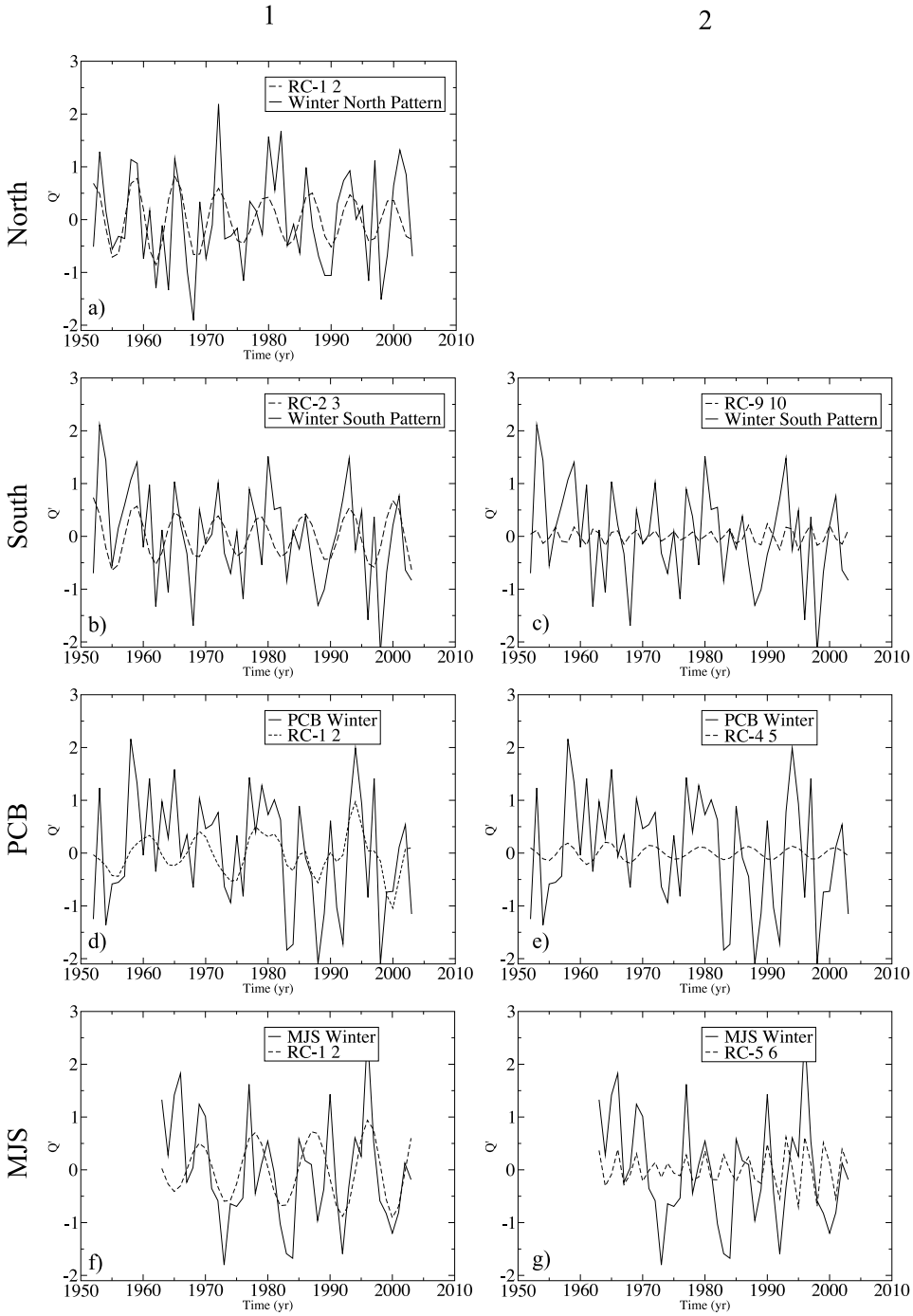

Figure 8. MTM reconstruction of SSA RCs for winter regional streamflow composites resulting from cluster analysis. Solid line shows original time series, and dashed line shows reconstruction based on pair of RCs as indicated in legend.

[29] Cluster analysis of 43 stream gages located in south central and southern Chile, between parallels 34°S and 40°S indicates that two major geographical zones can be considered homogeneous from the point of view of water availability variation. These zones include on one hand the greater Maule River basin and its tributaries (north) and on the other hand those rivers located within the Itata, Biobío, Imperial, and Valdivia river basins (south). On the basis of the clustering results, the Puelo River, located at the southern edge of the Los Lagos region, presents a more distinct hydrologic regime than that of the stations included in the south cluster. An additional station, MJS, was included in the analysis in order to assess patterns of temporal variability that could be representative of a large geographic region between 40°S and 45°S.

[30] Advanced time series analysis techniques were applied to the regional streamflow averages suggested by the clustering process. Correlation analysis with climatic for-

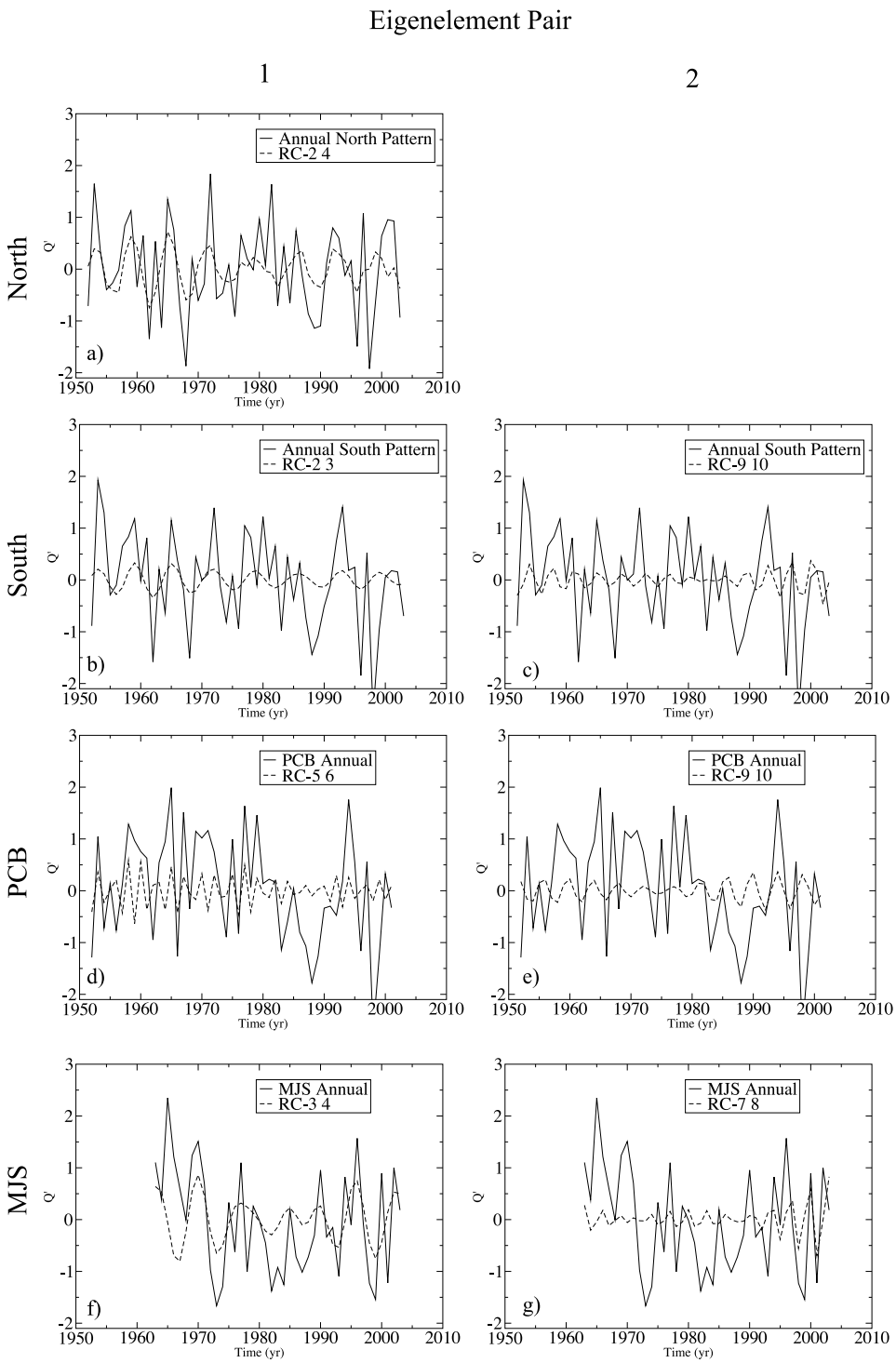

Figure 9. MTM reconstruction of SSA RCs for summer (January–February–March) regional streamflow composites resulting from cluster analysis. Solid line shows original time series, and dashed line shows reconstruction based on pair of RCs as indicated in legend.

cings reinforce previous findings in terms of a decreasing influence of ENSO over annual flows with southern latitude, which can be traced to a positive/negative correlation between annual and winter ENSO and winter/summer flows at the PCB station. We also found significant negative correlation between PDO as well as AAO and summer flows south of 37°S. This correlation explains, in view of phase changes of these two climatic forcings observed approximately after 1990, what can be interpreted as an increase in streamflow variability (particularly for summer, but also for mean annual flows) observed from the decomposition of the flow series into oscillating modes. Although certain changes in streamflow regime can be located around 1975, we found no conclusive evidence of this being related to the Pacific Shift [*Miller et al.*, 1994]. A more defined behavior was found in some PCs of the streamflow time series, where

decreasing trends were identified for all geographical regions at least at one temporal aggregation level (annual, winter, and summer). This is especially true for the south cluster (which shows decreasing annual, winter, and summer streamflow) and is consistent with decreasing trends in precipitation for this region reported in the literature. An additional identified feature was an increasing pattern found in Puelo and Mañihuales rivers after 1990, which is possibly related to a shift in AAO and PDO regimes around the same date. The fact that this increasing pattern appears in winter PCB but in summer MJS suggests a lagged effect, with at least 6 months difference, of the climatic or physiographic factors affecting streamflow production in these two basins. Lags, interactions, and other characteristic behavior of streamflow with respect to multiple climatic indexes and different time scales can be further studied using variations of the techniques shown here [e.g., *Dominguez and Kumar*, 2008; *Dominguez et al.*, 2008] and should be the subject of future work. Trend results should be interpreted with extreme caution in this context because of the available record limited length and also because of the high interannual variability affecting annual and seasonal streamflow. Nevertheless, the overall robustness of the clustering process for different seasons and time windows, together with the consistency between the time signals contained in the streamflow data and diverse climatic forcings, indicate that the patterns of variation shown here are plausible. The kind of analysis presented here has strong implications for water resource managers and planners because it represents in-depth analysis of underlying characteristics of river flows and their relation with global climate. This knowledge can be applied, for example, in (1) building better streamflow forecasting models with lags of a few months, and (2) going beyond the traditional hydrological engineering practice of computing flow duration curves and frequency analysis based on historical flows in order to characterize water availability at specific locations.

[31] This work was based on a large data set of discharge records that, while statistically comparable, correspond to a set of watersheds diverse in their physiographic characteristics. Future research should include efforts oriented to deepening our understanding of the physical controls of streamflow generation for selected watersheds in this ecoregion, in order to better predict the effect that projected changes in precipitation and temperature may have over water availability at different time scales.

[32] **Acknowledgments.** This research was supported by FONECYT grants 1050298 and 11060444. Support was also received from the Inter-American Institute for Global Change Research (IAI) through grant CRN II 2047, which is funded by the U.S. National Science Foundation (grant GEO-0452325). The authors wish to thank Dirección General de Aguas for providing the streamflow data, as well as C. Little and A. Lara for their thoughtful comments to an earlier version of this manuscript. Finally, the authors thank the three anonymous reviewers for their substantial help in making this a better article.

References

Aceituno, P. (1988), On the functioning of the Southern Oscillation in the South American sector: part I. Surface climate, *Mon. Weather Rev.*, *116* (3), 505–524, doi:10.1175/1520-0493(1988)116<0505:OTFOTS>2.0.CO;2.

Aceituno, P., et al. (1993), Climate along the extratropical west coast of South America, in *Earth Systems Responses to Global Change*, edited by H. A. Mooney et al., pp. 61–70, Academic, New York.

Allen, M. R., and L. A. Smith (1996), Monte Carlo SSA: Detecting irregular oscillations in the presence of colored noise, *J. Clim.*, *9*(12), 3373–3404, doi:10.1175/1520-0442(1996)009<3373:MCSDIO>2.0.CO;2.

Aravena, J. C., and B. H. Luckman (2009), Spatio-temporal rainfall patterns in southern South America, *Int. J. Climatol.*, *29*(14), 2106–2120, doi:10.1002/joc.1761.

Chen, J., et al. (2008), The spatiotemporal structure of 20th century climate variations in observations and reanalyses: part II. Pacific pan-decadal variability, *J. Clim.*, *21*, 2634–2650, doi:10.1175/2007JCLI2012.1.

Comisión Nacional de Medioambiente (2007), Estudio de la variabilidad climática en Chile para el siglo XXI, technical report, edited by Department of Geophysics, University of Chile, Santiago.

Dettinger, M. D., and H. F. Diaz (2000), Global characteristics of stream flow seasonality and variability, *J. Hydrometeorol.*, *1*(4), 289–310, doi:10.1175/1525-7541(2000)001<0289:GCOSFS>2.0.CO;2.

Dettinger, M. D., M. Ghil, C. M. Strong, W. Weibel, and P. Yiou (1995), Software expedites singular-spectrum analysis of noisy time series, *Eos Trans. AGU*, *76*(2), 12, 14, 21.

Dominguez, F., and P. Kumar (2008), Precipitation recycling variability and ecoclimatological stability—A study using NARR data: part I. Central USA plains ecoregion, *J. Clim.*, *21*(20), 5165–5186, doi:10.1175/2008JCLI1756.1.

Dominguez, F., P. Kumar, and E. Vivoni (2008), Precipitation recycling variability and ecoclimatological stability—A study using NARR data: part II. North American monsoon region, *J. Clim.*, *21*(20), 5187–5203, doi:10.1175/2008JCLI1760.1.

Fovell, R. G., and M. Y. C. Fovell (1993), Climate zones of the conterminous United States defined using cluster analysis, *J. Clim.*, *6*(11), 2103–2135, doi:10.1175/1520-0442(1993)006<2103:CZOTCU>2.0.CO;2.

Ghil, M., et al. (2002), Advanced spectral methods for climatic time series, *Rev. Geophys.*, *40*(1), 1003, doi:10.1029/2000RG000092.

Kresch, D. L. (1994), Variability of streamflow and precipitation in Washington, *U.S. Geol. Surv. Open File Rep., 93-4132*, 36 pp.

Lara, A., et al. (2008), A 400-year tree-ring record of the Puelo River summer-fall streamflow in the Valdivian rainforest eco-region, Chile, *Clim. Change*, *86*(3), 331–356, doi:10.1007/s10584-007-9287-7.

Mann, M. E., and J. M. Lees (1996), Robust estimation of background noise and signal detection in climatic time series, *Clim. Change*, *33*(3), 409–445, doi:10.1007/BF00142586.

Masiokas, M. H., et al. (2006), Snowpack variations in the central Andes of Argentina and Chile, 1951–2005: Large-scale atmospheric influences and implications for water resources in the region, *J. Clim.*, *19*(24), 6334–6352, doi:10.1175/JCLI3969.1.

Masiokas, M. H., et al. (2008), 20th-century glacier recession and regional hydroclimatic changes in northwestern Patagonia, *Global Planet. Change*, *60*(1–2), 85–100, doi:10.1016/j.gloplacha.2006.07.031.

McMahon, T. A. (1982), Hydrological characteristics of selected rivers of the world, *Tech. Doc. Hydrol., SC-82/WS/51*, 41 pp., United Nations Educ., Sci., and Cult. Organ., Paris.

Miller, A. J., et al. (1994), The 1976–77 climate shift of the Pacific Ocean, *Oceanography*, *7*(1), 21–26.

Montecinos, A., and P. Aceituno (2003), Seasonality of the ENSO-related rainfall variability in central Chile and associated circulation anomalies, *J. Clim.*, *16*(2), 281–296, doi:10.1175/1520-0442(2003)016<0281:SOTERR>2.0.CO;2.

Peña, H., et al. (1999), *Politica Nacional de Recursos Hidricos*, edited by D. G. Aguas, Minist. de Obras Publ., Santiago, Chile.

Penland, C., M. Ghil, and K. M. Weickmann (1991), Adaptive filtering and maximum entropy spectra with application to changes in atmospheric angular momentum, *J. Geophys. Res.*, *96*(D12), 22,659–22,671, doi:10.1029/91JD02107.

Percival, D. B., and A. T. Walden (1993), *Spectral Analysis for Physical Applications: Multitaper and Conventional Univariate Techniques*, Cambridge Univ. Press, New York.

Pezoa, L. S. (2003), Recopilación y análisis de la variación de las temperaturas (período 1965–2001) y las precipitaciones (período 1931–2001) a partir de la información de estaciones metereológicas de Chile entre los 33° y 53° de latitud sur, Univ. Austral de Chile, Valdivia.

Pittock, A. B. (1980), Patterns of climatic variation in Argentina and Chile: I. Precipitation, 1931–60, *Mon. Weather Rev.*, *108*(9), 1347–1361, doi:10.1175/1520-0493(1980)108<1347:POCVIA>2.0.CO;2.

Robertson, A. W. (1996), Interdecadal variability over the North Pacific in a multi-century climate simulation, *Clim. Dyn.*, *12*(4), 227–241, doi:10.1007/BF00219498.

Robertson, A. W., and C. R. Mechoso (1998), Interannual and decadal cycles in river flows of southeastern South America, *J. Clim.*, *11*(10),

2570–2581, doi:10.1175/1520-0442(1998)011<2570:IADCIR>2.0.CO;2.

Ropelewski, C. F., and M. S. Halpert (1989), Precipitation patterns associated with the high index phase of the Southern Oscillation, *J. Clim.*, *2*(3), 268–284, doi:10.1175/1520-0442(1989)002<0268:PPAWTH>2.0.CO;2.

Searcy, J. K., and C. H. Hardison (1960), Double mass curves, *U.S. Geol. Surv. Water Supply Pap., 1541-B*, 66 pp.

Smith, T. M., R. W. Reynolds, T. C. Peterson, and J. Lawrimore (2008), Improvements to NOAA's Historical Merged Land-Ocean Surface Temperature Analysis (1880–2006), *J. Clim.*, *21*, 2283–2296, doi:10.1175/2007JCLI2100.1.

Stahl, K., and S. Demuth (1999a), Linking streamflow drought to the occurrence of atmospheric circulation patterns, *Hydrol. Sci. J.*, *44*(3), 467–482, doi:10.1080/02626669909492240.

Stahl, K., and S. Demuth (1999b), *Methods for Regional Classification of Streamflow Drought Series: Cluster Analysis*, Univ. of Freiburg, Freiburg, Germany.

Thomson, D. J. (1990), Quadratic-inverse spectrum estimates: Applications to palaeoclimatology, *Philos. Trans. R. Soc. London, Ser. A*, *332*, 539–597.

Thompson, D. W. J., and J. M. Wallace (2000), Annular modes in the extratropical circulation: part I. Month-to-month variability, *J. Clim.*, *13*, 1000–1016, doi:10.1175/1520-0442(2000)013<1000:AMITEC>2.0.CO;2.

Vautard, R., and M. Ghil (1989), Singular spectrum analysis in nonlinear dynamics, with applications to paleoclimatic time series, *Physica D*, *35*(3), doi:10.1016/0167-2789(89)90077-8.

Vautard, R., et al. (1992), Singular-spectrum analysis: A toolkit for short, noisy chaotic signals, *Physica D*, *58*, 95–126.

Verdon, D. C., and S. W. Franks (2006), Long-term behavior of ENSO: Interactions with the PDO over the past 400 years inferred from paleoclimate records, *Geophys. Res. Lett.*, *33*, L06712, doi:10.1029/2005GL025052.

Villalba, R., et al. (2003), Large-scale temperature changes across the southern Andes: 20th-century variations in the context of the past 400 years, *Clim. Change*, *59*(1), 177–232, doi:10.1023/A:1024452701153.

Wilks, D. S. (2005), *Statistical Methods in the Atmospheric Sciences*, 648 pp., Elsevier, New York.

Zhang, Y., J. M. Wallace, and D. S. Battisti (1997), ENSO-like interdecadal variability: 1900–93, *J. Clim.*, *10*, 1004–1020, doi:10.1175/1520-0442(1997)010<1004:ELIV>2.0.CO;2.

J. McPhee and E. Rubio-Álvarez, Departamento de Ingeniería Civil, Facultad de Ciencias Físicas y Matemáticas, Universidad de Chile, Ave. Blanco Encalada 2002, Santiago 8370449, Chile. (jmcphee@ing.uchile.cl)